Climate model errors over the South Indian Ocean thermocline dome and their effect on the basin mode of interannual variability

Gen Li*

State Key Laboratory of Tropical Oceanography, South China Sea Institute of Oceanology, Chinese Academy of Sciences, Guangzhou, Guangdong, China

Shang-Ping Xie

Scripps Institution of Oceanography, University of California San Diego, La Jolla, California, USA; Physical Oceanography Laboratory, Ocean University of China, Qingdao, Shandong, China

Yan Du

State Key Laboratory of Tropical Oceanography, South China Sea Institute of Oceanology, Chinese Academy of Sciences, Guangzhou, Guangdong, China

**Corresponding author address*: Gen Li, State Key Laboratory of Tropical Oceanography, South China Sea Institute of Oceanology, CAS, 164 West Xingang Road, Guangzhou 510301, China. Email: ligen@scsio.ac.cn

ABSTRACT

An open-ocean thermocline dome south of the equator is a striking feature of the Indian Ocean (IO) as a result of equatorial westerly winds. Over the thermocline dome, the El Niño-forced Rossby waves help sustain the IO basin (IOB) mode and offer climate predictability for the IO and surrounding countries. This study shows that a common equatorial easterly wind bias, by forcing a westward-propagating downwelling Rossby wave in the South IO, induces too deep a thermocline dome over the southwestern IO (SWIO) in state-of-the-art climate models. Such a deep SWIO thermocline weakens the influence of subsurface variability on sea surface temperature, reducing the IOB amplitude and possibly limiting the models' skill of regional climate prediction. To the extent that the equatorial easterly wind bias originates from errors of the South Asian summer monsoon, improving the monsoon simulation can lead to substantial improvements in simulating and predicting interannual variability in the IO.

1. Introduction

The Indian Ocean (IO) is extraordinary in featuring westerly winds on the equator. The equatorial westerly winds are important for tropical IO climate (Schott et al. 2009). In particular, the cyclonic wind curl between the equatorial westerlies and southeasterly trades induces a pronounced open-ocean upwelling over the tropical southwestern IO (SWIO) (Xie et al. 2002). As a result, the shallow thermocline depth (20 °C isotherm, Z20) is present from 5° to 10°S and 50° to 80°E all through the year (Figure 1a and Figure S1 in the Supplementary Material), allowing a strong influence of subsurface variability on sea surface temperature (SST).

Such a SWIO thermocline dome is, in contrast to the tropical Pacific and Atlantic Oceans, unique to the IO with important implications for regional climate prediction (Xie et al. 2002). During El Niño, anomalous equatorial easterlies during boreal autumn (September-November, SON), one consequence of Walker circulation adjustments, force a westward-propagating downwelling Rossby wave in the tropical southeastern IO. As it propagates into the SWIO thermocline dome in the following boreal spring, the Rossby wave-induced SST warming there can, via initiating a series of air-sea interaction, help sustain the dominant mode of interannual variability for tropical IO SST (Du et al. 2009; Kosaka et al. 2013), i.e. the so-called the IO basin (IOB) mode (Klein et al. 1999; Lau et al. 2000), exerting important climate impacts affecting large populations in India, China, and Japan (Yang et al. 2007; Xie et al. 2009; Kosaka et al. 2013). Thus, the shallow thermocline dome and slow oceanic

Rossby wave south of the equator offer potential predictability of the IOB mode and IO rim countries' climate anomalies.

Most of the current coupled general circulation models (CGCMs) suffer from large simulation errors (Li and Xie 2012, 2014), for example, a strong easterly wind bias along the equatorial IO (Cai and Cowan 2013; Lee et al. 2013; Li et al. 2015) accompanied by physically consistent biases in SST and precipitation during SON, in patterns similar to a positive IO Dipole (IOD) (Saji et al. 1999; Webster et al. 1999) event in nature (Figure S2 in the Supplementary Material). Conceivably such a strong easterly wind bias in the equatorial IO in CGCMs could affect climate simulation off the equator. Given the importance of the SWIO thermocline dome for regional climate simulation and prediction, we propose a hypothesis now that the equatorial easterly bias in SON, in analogy to an El Niño forcing in nature, could deepen the SWIO thermocline dome and suppress the effect of subsurface thermocline variability on SST there in CGCMs. Indeed, the present study reveals that a too deep Z20 error over the SWIO is commonly present in the current CGCMs, owing to the typical equatorial easterly wind bias. We find that these mean state biases affect the simulated IOB amplitude of interannual variability, potentially limiting the skill of climate prediction using CGCMs.

The rest of the paper is organized as follows. Section 2 describes models and datasets used in this study. Section 3 investigates the SWIO thermocline dome errors

and their effects on the simulation and prediction of interannual IOB variability in CGCMs. Section 4 is a summary with discussion.

2. Models and datasets

We examine the 56-yr (1950-2005) climate of the historical simulations from 19 CGCMs in the Coupled Model Intercomparison Projection phase 5 (CMIP5) multi-model ensemble (Taylor et al. 2012). Table S1 in the Supplementary Material lists these models. The description of individual models can be obtained online at http://www-pcmdi.llnl.gov/. The multi-model ensemble mean (MME) in this study is defined as only the average of 14 CGCMs [excluding 5 CGCMs (red circled group in Figure S2 in the Supplementary Material) with no equatorial easterly wind bias], unless otherwise specified.

For comparison, we also examine both the observed and reanalyzed (assimilated) datasets (for simplicity referred to as observations) including the ocean temperature from the Simple Ocean Data Assimilation (SODA) reanalysis (Carton et al. 2008) for 1950-99, Hadley Centre Sea Ice and SST (HadISST; Rayner et al. 2003) for 1950-99, precipitation from the Global Precipitation Climatology Project (GPCP; Adler et al. 2003) for 1979-2008, and lower tropospheric (925 mb) wind from ECWMF 40 Year Re-analysis (ERA-40; Uppala et al. 2005) for 1958-2001.

3. Results

a. Thermocline dome errors

Figures 1a and 1b compare the annual mean Z20 over the tropical IO between observations and the MME simulation. The models have an overly deep thermocline dome over the SWIO, with the area surrounded by 100 m contours of annual mean Z20 in the MME simulation greatly shrinking into less than half of that in observations. While the annual mean Z20 over the SWIO thermocline dome (5°-10°S, 50°-80°E) in observations is only about 90 m depth, that in the MME simulation is significantly deepened and reaches up to about 105 m depth (Figure 1c). In general, too deep a thermocline dome over the SWIO in CMIP5 CGCMs is largely independent of season, but the bias amplitudes can vary with season, with being slightly weaker in magnitude in boreal summer (June-August, JJA; Figure S1 in the Supplementary Material).

b. Origin of the thermocline dome errors

We turn our attention to the cause of Z20 deepening error over the SWIO thermocline dome in CMIP5 CGCMs. Figure 2 presents the inter-model regressions of SST, Z20, and 925 mb wind onto the central equatorial IO (CEIO, 70°-90°E) zonal wind during boreal autumn among observations and 19 CMIP5 CGCMs. Associated with the strong easterly wind bias on the equator, the cyclonic wind curl between the equatorial westerlies and southeasterly trades and resultant open-ocean upwelling in

the tropical South IO would be largely weakened in CMIP5 CGCMs, deepening the thermocline there.

Then, the Z20 biases averaged in 8°-12°S as a function of longitude and calendar month for the MME simulation in comparison with observations are shown in Figure 3. Accompanied by the strong equatorial easterly wind bias, the thermocline deepening error in the MME simulation grows rapidly from September to November at 80°-85°E with a maximum being more than 30 m, which thereafter propagates slowly to the west and reaches 60°E in May of the following year. Such a westward propagation of thermocline deepening bias along 10°S in CMIP5 CGCMs is similar to the South IO Rossby wave response to El Niño-forced easterly wind anomalies along the equatorial IO in nature (Xie et al. 2002).

Inter-model statistics also support our hypothesis that such a deepening SWIO thermocline dome originates from too strong equatorial easterly wind bias in CGCMs. Figures 4a and 4b show the inter-model relationship of the CEIO zonal wind in SON with the Z20 averaged over the SWIO thermocline dome in SON and boreal winter (December-February, DJF) among observations and 19 CMIP5 CGCMs, respectively. Indeed, models with a weaker equatorial westerly wind in SON tend to feature a deeper thermocline over the SWIO in both SON and DJF, with the inter-model correlations at -0.71 and -0.76, respectively.

c. Effects on the basin mode

Finally, our concern is the effects of such a deep SWIO thermocline dome in CMIP5 CGCMs induced by the equatorial easterly wind bias on the regional climate simulation and prediction on interannual time scale. As explained in the Introduction, if properly initialized, CGCMs can potentially predict the El Niño-forced IOB mode and hence IOB-related regional climate anomalies in advance, owing to the shallow thermocline dome and slow oceanic Rossby waves in the tropical South IO. However, too deep a thermocline dome over the SWIO in CMIP5 CGCMs results in significantly lower correlations between interannual variability in Z20 and SST there from November to May in comparison with observations, i.e. a significantly weak influence of subsurface thermocline variability on SST (Figure 5).

As a result, importantly, this restrained thermocline-SST feedback in the tropical South IO would lead to an underestimation for the IOB amplitude of interannual variability in CGCMs and also inevitably limit their skill of regional climate prediction. Here the IOB amplitude is defined as the interannual standard deviation of tropical IO (40°-110°E, 20°S-20°N) mean SST during February-August; and the predictability of the IOB warming following El Niño is characterized by the correlation coefficient between the Nino3 (5°S-5°N, 150°-90°W) SST index during October-December and tropical IO mean SST during February-August of the following year. Indeed, models with a stronger equatorial easterly wind bias in SON tend to have a less amplitude of interannual IOB variability (Figure 4c) and weaker

predictability of the IOB warming following El Niño (Figure 4d), with the inter-model correlations of 0.76 and 0.72, respectively.

4. Summary and discussion

The equatorial westerly winds are the unique observed phenomenon to the IO, inducing a thermocline dome south of the equator (Xie et al. 2002). The shallow SWIO thermocline plays an important role for shaping tropical IO climate and its variability. For instance, its interaction with the El Niño-forced South IO oceanic Rossby wave can help sustain the IOB mode of inter-annual variability by initiating a series of air-sea interaction (Du et al. 2009; Kosaka et al. 2013), providing potential climate predictability in the region (Yang et al. 2007; Xie et al. 2009; Chowdary et al. 2010). However, the westerly wind over the equatorial IO is too weak during SON in most CMIP5 CGCMs. The equatorial easterly wind bias in CMIP5 CGCMs causes too deep a SWIO thermocline dome through inducing a westward-propagating downwelling Rossby wave in the tropical South IO, somewhat similar to a South IO oceanic Rossby wave response to El Niño-forced easterly wind anomalies along the equator in nature. The deep thermocline dome bias over the SWIO in CMIP5 CGCMs could significantly reduce the effect of subsurface thermocline variability on SST there. As a result, too weak a thermocline-SST feedback over the SWIO in CMIP5 CGCMs results in a deficiency in the simulated amplitude for the IOB mode of

interannual variability, and also lowers their skill in predicting the IOB warming following El Niño.

The recent studies (Cai et al. 2013; Li et al. 2015) find that the easterly wind error in CGCMs can result in a too steep eastward shoaling of thermocline in the equatorial IO (Figure S3 in the Supplementary Material). The unrealistically steep thermocline slope generates too strong a thermocline feedback on SST, and thus develops an excessively large IOD amplitude of inter-annual variability in CGCMs (Cai and Cowan 2013), exerting profound social and economic consequences for the IO rim countries such as Indonesia and Kenya (Saji et al. 1999; Hashizume et al. 2009; Cai et al. 2011). Furthermore, our recent research (Li et al. 2015) suggests that the equatorial easterly wind bias can be traced back to errors in the South Asian summer monsoon. Too weak cross-equatorial monsoon over the western basin in JJA (Annamalai et al. 2007; Boos and Hurley 2013) causes a sustained warm SST bias in the western equatorial IO (Figure S3 in the Supplementary Material). In SON, Bjerknes feedback helps amplify this SST error into an IOD-like pattern, with a strong equatorial easterly bias accompanied by physically consistent bias in the precipitation dipole (Figure S2 in the Supplementary Material). These results imply that reducing the monsoon errors in CGCMs will improve climate simulation and prediction for the IO and rim countries, and increase our confidence in their application for regional climate projection.

Acknowledgements. This work was supported by the National Basic Research Program of China (Grants 2012CB955603 and 2010CB950302), the Natural Science Foundation of China (Grant 41406026), the Pearl River Nova Program of Guangzhou, the Technology Foundation for Selected Overseas Chinese Scholars (Ministry of Human Resources and Social Security of the People's Republic of China), the US National Science Foundation, and the CAS/SAFEA International Partnership Program for Creative Research Teams. We also wish to thank the climate modeling groups (Table S1 in the Supplementary Material) for producing and making available their model output, the WCRP's Working Group on Coupled Modeling (WGCM) for organizing the CMIP5 analysis activity, the Program for Climate Model Diagnostics and Intercomparison (PCMDI) for collecting and archiving the CMIP5 multi-model data, and the Office of Science, U.S. Departmentof Energy for supporting these datasets in partnership with the Global Organization for Earth System Science Portals.

REFERENCES

Adler, R. F., and Coauthors, 2003: The version 2 global precipitation climatology project (GPCP) monthly precipitation analysis (1979-present). *J. Hydrometeor.,* **4,** 1147–1167.

Annamalai, H., K. Hamilton, and K. R. Sperber, 2007: The South Asian summer monsoon and its relationship with ENSO in the IPCC AR4 simulations. *J. Climate,* **20,** 1071–1092.

Boos, W. R., and J. V. Hurley, 2013: Thermodynamic bias in the multimodel mean boreal summer monsoon. *J. Climate,* **26,** 2279–2287.

Cai, W., and T. Cowan, 2013: Why is the amplitude of the Indian Ocean Dipole overly large in CMIP3 and CMIP5 climate models? *Geophys. Res. Lett.*, **40,** 1200–1205.

Cai, W., A. Sullivan, T. Cowan, J. Ribbe, and G. Shi, 2011: Simulation of the Indian Ocean Dipole: A relevant criterion for selecting models for climate projections. *Geophys. Res. Lett.,* **38,** L03704, doi:10.1029/2010GL046242.

Carton, J. A., and B. S. Giese, 2008: A reanalysis of Ocean climate using simple Ocean data assimilation (SODA). *Mon. Wea. Rev.,* **136,** 2999–3017.

Chowdary, J. S., S.-P. Xie, J.-Y. Lee, Y. Kosaka, and B. Wang, 2010: Predictability of summer Northwest Pacific climate in eleven coupled model hindcasts: Local and remote forcing. *J. Geophys. Res.,* **115,** D22121, doi:10.1029/2010JD014595.

Du, Y., S.-P. Xie, G. Huang, and K. Hu, 2009: Role of air-sea interaction in the long persistence of El Niño-induced North Indian Ocean warming. *J. Climate*, **22,** 2023–2038.

Hashizume, M., T. Terao, and N. Minakawa, 2009: The Indian Ocean Dipole and malaria risk in the highlands of western Kenya. *Proc. Natl. Acad. Sci. USA,* **106,** 1857–1862.

Klein, S. A., B. J. Soden, and N.-C. Lau, 1999: Remote sea surface temperature variations during ENSO: Evidence for a tropical atmospheric bridge. *J. Climate,* **12,** 917–932.

Kosaka, Y., S.-P. Xie, N.-C. Lau, and G. A. Vecchi, 2013: Origin of seasonal predictability for summer climate over the Northwestern Pacific. *Proc. Natl. Acad. Sci. USA,* **110,** 7574–7579.

Lau, N.-C., and M. J. Nath, 2000: Impact of ENSO on the variability of the Asian-Australian monsoons as simulated in GCM experiments. *J. Climate,* **13,** 4287–4309.

Lee, T., D. E. Waliser, J.-L. F. Li, F. W. Landerer, and M. M. Gierach, 2013: Evaluation of CMIP3 and CMIP5 wind stress climatology using satellite measurements and atmospheric reanalysis products. *J. Climate,* **26,** 5810–5826.

Li, G., and S.-P. Xie, 2012: Origins of tropical-wide SST biases in CMIP multi-model ensembles. *Geophys. Res. Lett.,* **39,** L22703, doi:10.1029/2012GL053777.

Li, G., and S.-P. Xie, 2014: Tropical biases in CMIP5 multimodel ensemble: The excessive equatorial Pacific cold tongue and double ITCZ problems. *J. Climate*, **27,** 1765–1780.

Li, G., S.-P. Xie, and Y. Du, 2015: Monsoon-induced biases of climate models over the tropical Indian Ocean. *J. Climate*, doi: http://dx.doi.org/10.1175/JCLI-D-14-00810.1, in press.

Rayner, N. A., D. E. Parker, E. B. Horton, C. K. Folland, L. V. Alexander, D. P. Rowell, E. C. Kent, and A. Kaplan, 2003: Global analyses of sea surface temperature, sea ice, and night marine air temperature since the late nineteenth century. *J. Geophys. Res.*, **108,** 4407, doi:10.1029/2002JD002670.

Saji, N. H., B. N. Goswami, P. N. Vinayachandran, and T. Yamagata, 1999: A dipole mode in the tropical Indian Ocean. *Nature*, **401,** 360–363.

Schott, F. A., S.-P. Xie, and J. P. McCreary, 2009: Indian Ocean circulation and climate variability. *Rev. Geophys.*, **47,** RG1002, doi:10.1029/2007RG000245.

Taylor, K. E., J. S. Ronald, and G. A. Meehl, 2012: An overview of CMIP5 and the experiment design. *Bull. Amer. Meteor. Soc.*, **93,** 485–498.

Uppala, S. M., and Coauthors, 2005: The ERA-40 re-analysis. *Q. J. R. Meteor. Soc.*, **131,** 2961–3012.

Webster, P. J., A. M. Moore, J. P. Loschnigg, and R. R. Leben, 1999: Coupled ocean-atmosphere dynamics in the Indian Ocean during 1997-98. *Nature*, **401,** 356–360.

Xie, S.-P., H. Annamalai, F. A. Schott, and J. P. McCreary, 2002: Structure and mechanisms of South Indian Ocean climate variability. *J. Climate,* **15,** 864–878.

Xie, S.-P., K. Hu, J. Hafner, H. Tokinaga, Y. Du, G. Huang, and T. Sampe, 2009: Indian Ocean capacitor effect on Indo-western Pacific climate during the summer following El Niño. *J. Climate*, **22,** 730–747.

Yang, J., Q. Liu, S.-P. Xie, Z. Liu, and L. Wu, 2007: Impact of the Indian Ocean SST basin mode on the Asian summer monsoon. *Geophys. Res. Lett.,* **34,** L02708, doi:10.1029/2006GL028571.

Figure captions

Figure 1. Annual mean distributions of thermocline depth (20 °C isotherm, Z20; units: m) in (a) observations and (b) the multi-model ensemble mean (MME) simulation; (c) Z20 averaged over the SWIO thermocline dome (50°-80°E, 5°-10°S) for observations and the MME simulation. The 100 m contours in (a) and (b) are denoted by the black solid curves; the observed 100 m contours in (b) are superimposed in white dashed curves. The error bar in (c) indicates the standard deviation spread among CGCMs.

Figure 2. Inter-model regressions of SST (color shaded, °C), Z20 (contours, m), and 925 mb wind (vectors, m/s) during October-November onto the central equatorial IO (CEIO, 70°-90°E) zonal wind in SON among observations and 19 CMIP5 CGCMs.

Figure 3. Longitude-time section of MME biases for Z20 (contours; shade > 15 m) averaged in 8°-12°S and equatorial zonal wind (vectors in m/s) in the CMIP5 CGCMs. The wind speed smaller than 1 m/s has been masked out.

Figure 4. Scatter plots of the CEIO zonal wind (m/s) in SON versus (a) Z20 (m) over the SWIO thermocline dome in SON, (b) SWIO Z20 in December-February (DJF), (c) IOB amplitude, and (d) predictability of the IOB warming following El Niño among observations and 19 CMIP5 CGCMs. The IOB amplitude is here defined as the interannual standard deviation of tropical IO (40°-110°E, 20°S-20°N) mean SST (°C)

during February-August. The predictability of the IOB warming following El Niño is characterized by the correlation between the Nino3 (5°S-5°N, 150°-90°W) SST index during October-December and tropical IO mean SST during February-August of the following year. The inter-model correlation (r) is shown in each panel.

Figure 5. The correlations between interannual variability in Z20 and SST over the SWIO thermocline dome for observations versus the MME as a function of calendar month. The error bars indicate the standard deviation spread among CGCMs.

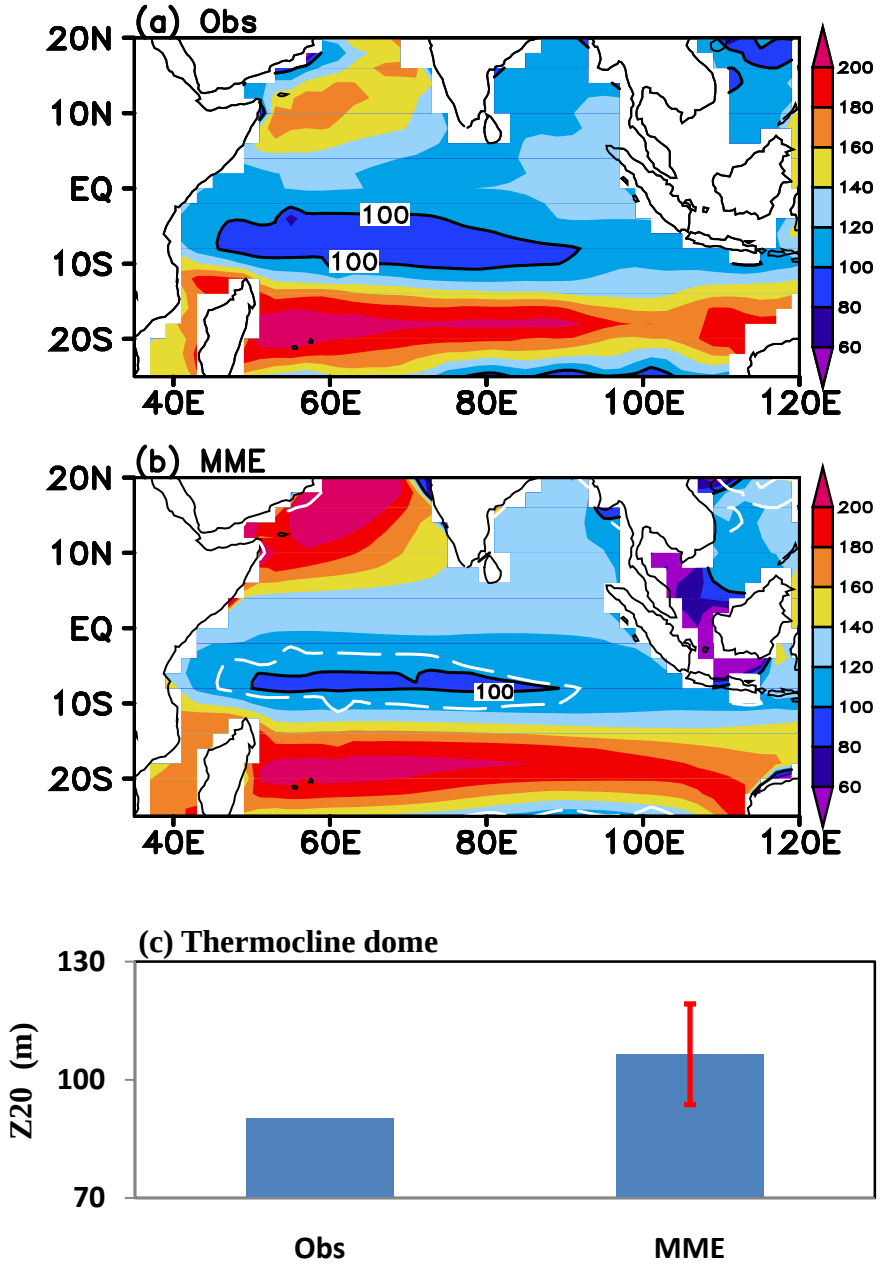

Figure 1. Annual mean distributions of thermocline depth (20 °C isotherm, Z20; units: m) in (a) observations and (b) the multi-model ensemble mean (MME) simulation; (c) Z20 averaged over the SWIO thermocline dome (50°-80°E, 5°-10°S) for observations and the MME simulation. The 100 m contours in (a) and (b) are denoted by the black solid curves; the observed 100 m contours in (b) are superimposed in white dashed curves. The error bar in (c) indicates the standard deviation spread among CGCMs.

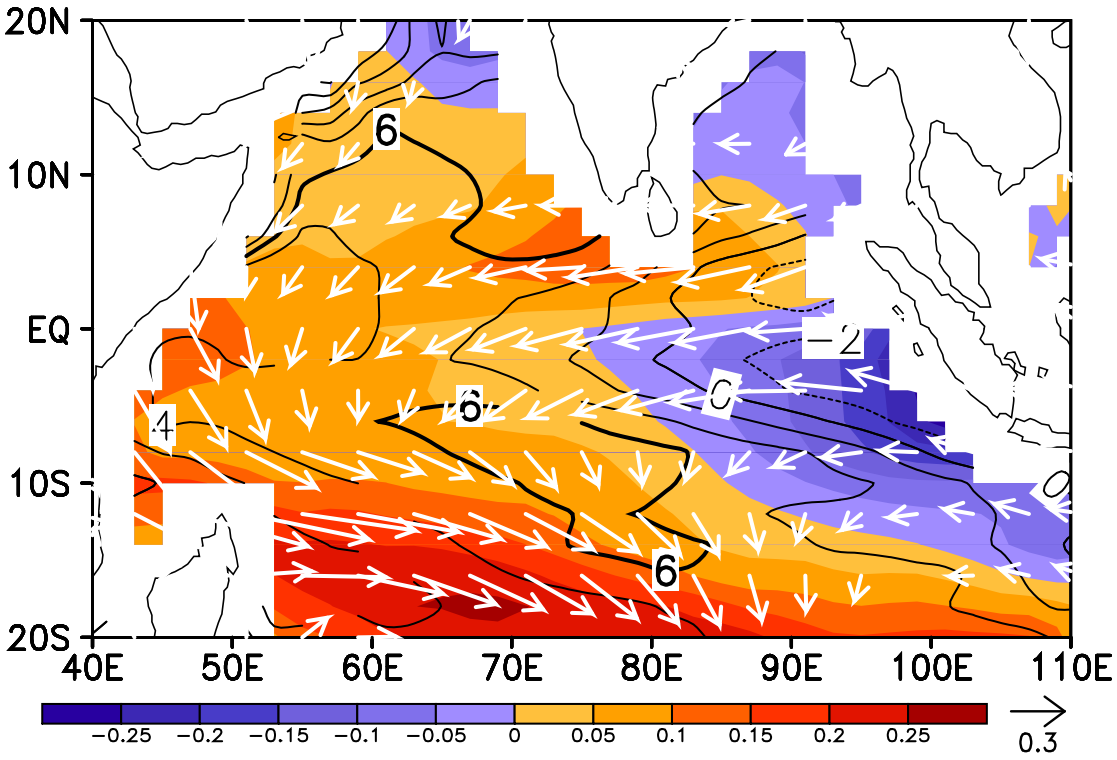

Figure 2. Inter-model regressions of SST (color shaded, °C), Z20 (contours, m), and 925 mb wind (vectors, m/s) during October-November onto the central equatorial IO (CEIO, 70°-90°E) zonal wind in SON among observations and 19 CMIP5 CGCMs.

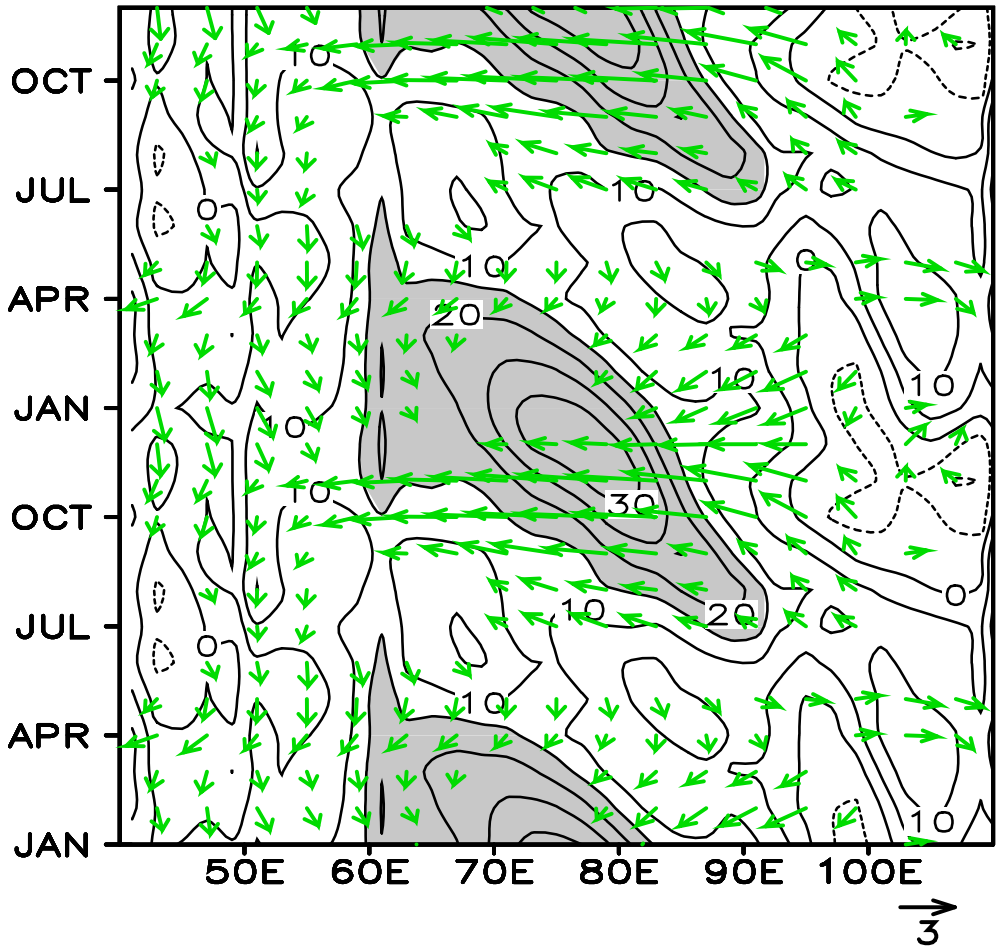

Figure 3. Longitude-time section of MME biases for Z20 (contours; shade > 15 m) averaged in 8°-12°S and equatorial zonal wind (vectors in m/s) in the CMIP5 CGCMs. The wind speed smaller than 1 m/s has been masked out.

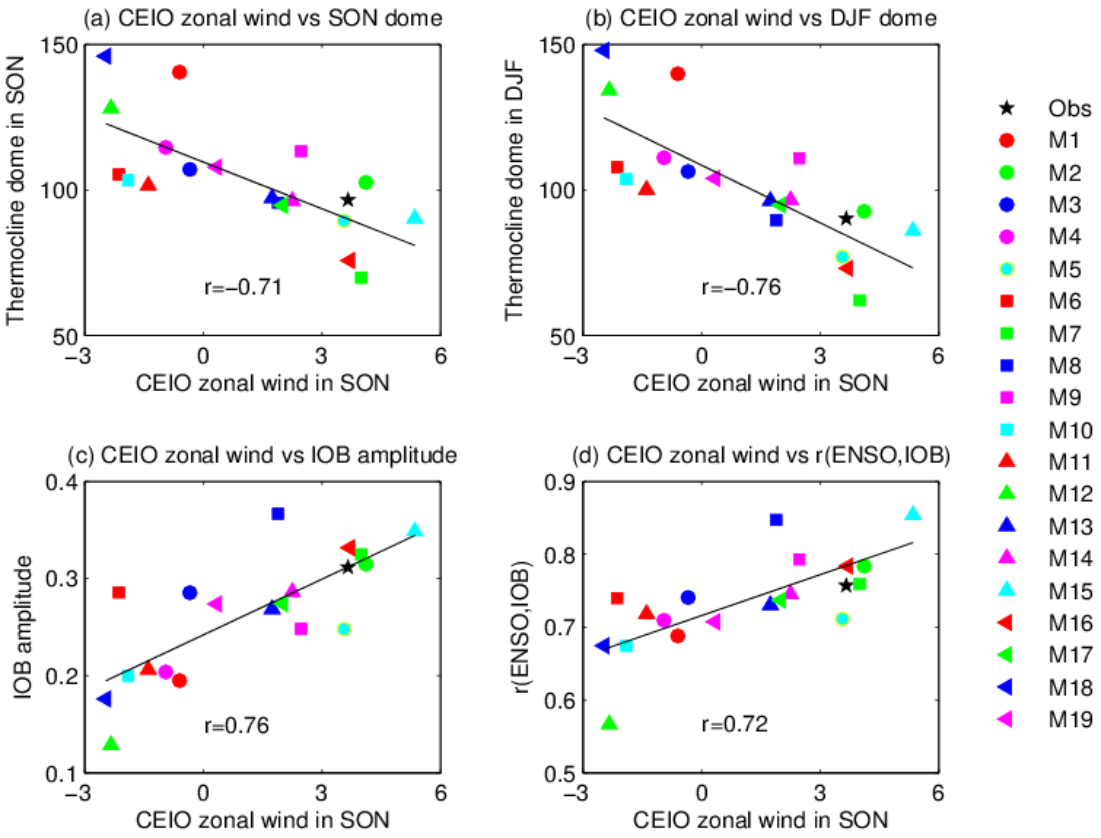

Figure 4. Scatter plots of the CEIO zonal wind (m/s) in SON versus (a) Z20 (m) over the SWIO thermocline dome in SON, (b) SWIO Z20 in December-February (DJF), (c) IOB amplitude, and (d) predictability of the IOB warming following El Niño among observations and 19 CMIP5 CGCMs. The IOB amplitude is here defined as the interannual standard deviation of tropical IO (40°-110°E, 20°S-20°N) mean SST (°C) during February-August. The predictability of the IOB warming following El Niño is characterized by the correlation between the Nino3 (5°S-5°N, 150°-90°W) SST index during October-December and tropical IO mean SST during February-August of the following year. The inter-model correlation (r) is shown in each panel.

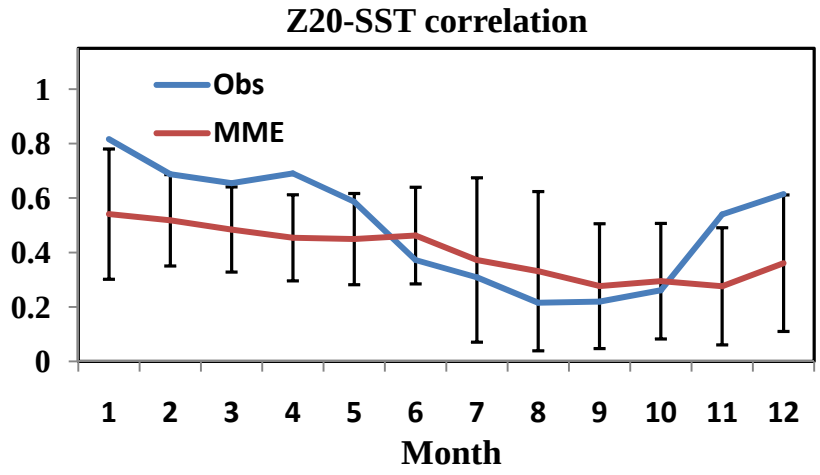

Figure 5. The correlations between interannual variability in Z20 and SST over the SWIO thermocline dome for observations versus the MME as a function of calendar month. The error bars indicate the standard deviation spread among CGCMs.